

[Extended version] Rethinking Deep Neural Network Ownership Verification: Embedding Passports to Defeat Ambiguity Attacks

Lixin Fan¹ Kam Woh Ng² Chee Seng Chan²

¹WeBank AI Lab, Shenzhen, China

²Center of Image and Signal Processing, Faculty of Comp. Sci. and Info., Tech.

University of Malaya, Kuala Lumpur, Malaysia

{lixinfan@webank.com; kamwoh@siswa.um.edu.my; cs.chan@um.edu.my}

Abstract—With substantial amount of time, resources and human (team) efforts invested to explore and develop successful deep neural networks (DNN), there emerges an urgent need to protect these inventions from being illegally copied, redistributed, or abused without respecting the intellectual properties of legitimate owners. Following recent progresses along this line, we investigate a number of watermark-based DNN ownership verification methods in the face of ambiguity attacks, which aim to cast doubts on the ownership verification by forging counterfeit watermarks. It is shown that ambiguity attacks pose serious threats to existing DNN watermarking methods. As remedies to the above-mentioned loophole, this paper proposes novel *passport*-based DNN ownership verification schemes which are both *robust to network modifications* and *resilient to ambiguity attacks*. The gist of embedding digital passports is to design and train DNN models in a way such that, the DNN inference performance of an original task will be significantly *deteriorated due to forged passports*. In other words, genuine passports are not only verified by looking for the predefined signatures, but also reasserted by the *unyielding DNN model inference performances*. Extensive experimental results justify the effectiveness of the proposed passport-based DNN ownership verification schemes. Code and models are available at <https://github.com/kamwoh/DeepIPR>

I. INTRODUCTION

With the rapid development of deep neural networks (DNN), Machine Learning as a Service (MLaaS) has emerged as a viable and lucrative business model. However, building a successful DNN is not a trivial task, which usually requires substantial investments on expertise, time and resources. As a result of this, there is an urgent need to protect invented DNN models from being illegally copied, redistributed or abused (i.e. intellectual property infringement). Recently, for instance, digital *watermarking* techniques have been adopted to provide such a protection, by embedding watermarks into DNN models during the training stage. Subsequently, ownerships of these inventions are verified by the detection of the embedded watermarks, which are supposed to be robust to multiple types of modifications such as model fine-tuning, model pruning and watermark overwriting [1], [2], [3], [4].

In terms of deep learning methods to embed watermarks, existing approaches can be broadly categorized into two schools: a) the *feature-based* methods that embed designated watermarks into the DNN weights by imposing additional regularization

terms [1], [3], [5]; and b) the *trigger-set* based methods that rely on adversarial training samples with specific labels (i.e. backdoor trigger sets) [2], [4]. Watermarks embedded with either of these methods have successfully demonstrated robustness against *removal attacks* which involve modifications of the DNN weights such as *fine-tuning* or *pruning*. However, our studies disclose the existence and effectiveness of *ambiguity attacks* which aim to cast doubt on the ownership verification by *forging additional watermarks* for DNN models in question (see Fig. 1). We also show that *it is always possible to reverse-engineer forged watermarks at minor computational cost* where the original training dataset is also not needed (Sect. II).

As remedies to the above-mentioned loophole, this paper proposes a novel *passport*-based approach. There is a unique advantage of the proposed passports over traditional watermarks - i.e. the inference performance of a pre-trained DNN model will either *remain intact* given the presence of valid passports, or be *significantly deteriorated* due to either the modified or forged passports. In other words, we propose to *modulate the inference performances* of the DNN model depending on the presented passports, and by doing so, one can develop ownership verification schemes that are both *robust to removal attacks* and *resilient to ambiguity attacks* at once (Sect. III).

The contributions of our work are threefold: i) we put forth a general formulation of DNN ownership verification schemes and, empirically, we show that existing DNN watermarking methods are vulnerable to ambiguity attacks; ii) we propose novel passport-based verification schemes and demonstrate with extensive experiment results that these schemes successfully defeat ambiguity attacks; iii) methodology-wise, the proposed modulation of DNN inference performance based on the presented passports (Eq. 5) plays an indispensable role in bringing the DNN model behaviours under control against adversarial attacks.

A. Related work

Uchida et. al [1] was probably the first work that proposed to embed watermarks into DNN models by imposing an additional *regularization term* on the weights parameters. [2], [6] proposed to embed watermarks in the classification labels

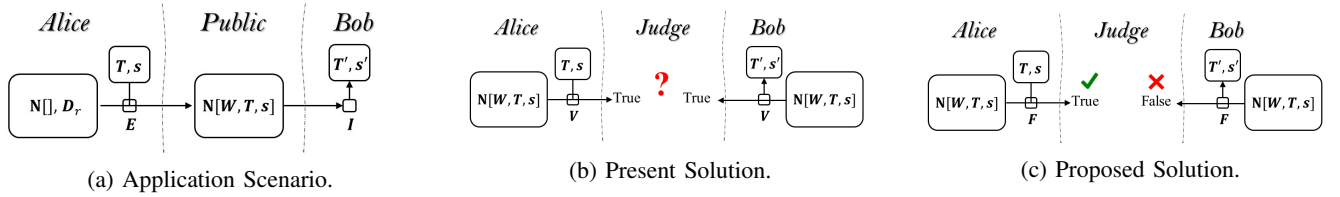


Fig. 1: DNN model ownership verification in the face of ambiguity attacks. (a): Owner *Alice* uses an embedding process E to train a DNN model with watermarks (\mathbf{T}, s) and releases the model publicly available; Attacker *Bob* forges counterfeit watermarks (\mathbf{T}', s') with an invert process I ; (b): The ownership is in doubt since both the original and forged watermarks are detected by the verification process V (Sect. II-B); (c): The ambiguity is resolved when our proposed passports are embedded and the network performances are evaluated in favour of the original passport by the fidelity evaluation process F (See Definition 1 and Sect. III-D).

of adversarial examples in a *trigger set*, so that the watermarks can be extracted remotely through a service API without the need to access the network weights (i.e. black-box setting). Also in both black-box and white box settings, [3], [5], [7] demonstrated how to embed watermarks (or fingerprints) that are robust to various types of attacks. In particular, it was shown that embedded watermarks are in general robust to *removal attacks* that modify network weights via fine-tuning or pruning. Watermark overwriting, on the other hand, is more problematic since it aims to simultaneously embed a new watermark and destroy the existing one. Although [5] demonstrated robustness against overwriting attack, it did not resolve the ambiguity resulted from the counterfeit watermark. Adi et al. [2] also discussed how to deal with an adversary who fine-tuned an already watermarked networks with new trigger set images. Nevertheless, [2] required the new set of images to be distinguishable from the true trigger set images. This requirement is however often unfulfilled in practice, and our experiment results show that none of existing watermarking methods are able to deal with ambiguity attacks explored in this paper (see Sect. II).

In the context of digital image watermarking, [8], [9] have studied *ambiguity attacks* that aim to create an ambiguous situation in which a watermark is reverse-engineered from an already watermarked image, by taking advantage of the invertibility of forged watermarks [10]. It was argued that *robust watermarks do not necessarily imply the ability to establish ownership*, unless *non-invertible watermarking* schemes are employed (see Proposition 2 for our proposed solution).

II. RETHINKING DEEP NEURAL NETWORK OWNERSHIP VERIFICATION

This section analyses and generalizes existing DNN watermarking methods in the face of ambiguity attacks. We must emphasize that the analysis mainly focuses on three aspects i.e. *fidelity*, *robustness* and *invertibility* of the ownership verification schemes, and we refer readers to representative previous work [1], [2], [3], [4] for formulations and other desired features of the entire watermark-based intellectual property (IP) protection schemes, which are out of the scope of this paper.

A. Reformulation of DNN ownership verification schemes

Figure 1 summarizes the application scenarios of DNN model ownership verifications provided by the watermark based schemes. Inspired by [10], we also illustrate an ambiguous situation in which rightful ownerships cannot be uniquely resolved by the current watermarking schemes alone. This loophole is largely due to an intrinsic weakness of the watermark-based methods i.e. *invertibility*. Formally, the definition of DNN model ownership verification schemes is generalized as follows.

Definition 1. A DNN model ownership verification scheme is a tuple $\mathcal{V} = (E, F, V, I)$ of processes:

- I) An *embedding* process $E(\mathbf{D}_r, \mathbf{T}, s, \mathbb{N}[\cdot, L]) = \mathbb{N}[\mathbf{W}, \mathbf{T}, s]$, is a DNN learning process that takes *training data* $\mathbf{D}_r = \{\mathbf{X}_r, \mathbf{y}_r\}$ as inputs, and optionally, either trigger set data $\mathbf{T} = \{\mathbf{X}_T, \mathbf{y}_T\}$ or signature s , and outputs the model $\mathbb{N}[\mathbf{W}, \mathbf{T}, s]$ by minimizing a given loss L .

Remark: the DNN architectures are pre-determined by $\mathbb{N}[\cdot]$ and, after the DNN weights \mathbf{W} are learned, either the trigger set \mathbf{T} or signatures s will be embedded and can be verified by the verification process defined next¹.

- II) A *fidelity evaluation* process $F(\mathbb{N}[\mathbf{W}, \cdot, \cdot], \mathbf{D}_t, \mathcal{M}_t, \epsilon_f) = \{True, False\}$ is to evaluate whether or not the discrepancy is less than a pre-defined threshold i.e. $|\mathcal{M}(\mathbb{N}[\mathbf{W}, \cdot, \cdot], \mathbf{D}_t) - \mathcal{M}_t| \leq \epsilon_f$, in which $\mathcal{M}(\mathbb{N}[\mathbf{W}, \cdot, \cdot], \mathbf{D}_t)$ is the DNN inference performance tested against a set of *test data* \mathbf{D}_t where \mathcal{M}_t is the target inference performance.

Remark: it is often expected that a well-behaved embedding process will not introduce a significant inference performance change that is greater than a predefined threshold ϵ_f . Nevertheless, this fidelity condition remains to be verified for DNN models under either removal attacks or ambiguity attacks.

- III) A *verification* process $V(\mathbb{N}[\mathbf{W}, \cdot, \cdot], \mathbf{T}, s, \epsilon_s) = \{True, False\}$ checks whether or not the expected signature s or trigger set \mathbf{T} is successfully verified for a given DNN model $\mathbb{N}[\mathbf{W}, \cdot, \cdot]$.

¹Learning hyper-parameters such as learning rate and the type of optimization methods are considered irrelevant to ownership verifications, and thus they are not included in the formulation.

Remark: for feature-based schemes, V involves the detection of embedded signatures $s = \{\mathbf{P}, \mathbf{B}\}$ with a false detection rate that is lesser than a predefined threshold ϵ_s . Specifically, the detection boils down to measure the distances $D_f(f_e(\mathbf{W}, \mathbf{P}), \mathbf{B})$ between target feature \mathbf{B} and features extracted by a transformation function $f_e(\mathbf{W}, \mathbf{P})$ parameterized by \mathbf{P} .

Remark: for trigger-set based schemes, V first invokes a DNN inference process that takes trigger set samples \mathbf{T}_x as inputs, and then it checks whether the prediction $f(\mathbf{W}, \mathbf{X}_T)$ produces the designated labels \mathbf{T}_y with a false detection rate that is lesser than a threshold ϵ_s .

IV) An *invert* process $I(\mathbb{N}[\mathbf{W}, \mathbf{T}, s]) = \mathbb{N}[\mathbf{W}, \mathbf{T}', s']$ exists and constitutes a successful *ambiguity attack*, if

- a set of new trigger set \mathbf{T}' and/or signature s' can be reverse-engineered for a given DNN model;
- the forged \mathbf{T}', s' can be successfully verified with respect to the given DNN weights \mathbf{W} i.e. $V(I(\mathbb{N}[\mathbf{W}, \mathbf{T}, s]), \mathbf{T}', s', \epsilon_s) = \text{True}$;
- the fidelity evaluation outcome $F(\mathbb{N}[\mathbf{W}, \cdot, \cdot], \mathbf{D}_t, \mathcal{M}_t, \epsilon_f)$ defined in Definition 1.II remains *True*.

Remark: this condition plays an indispensable role in designing the non-invertible verification schemes to defeat ambiguity attacks (see Sect. III-D).

V) If at least one invert process exists for a DNN verification scheme \mathcal{V} , then the scheme is called an *invertible* scheme and denoted by $\mathcal{V}^I = (E, F, V, I \neq \emptyset)$; otherwise, the scheme is called *non-invertible* and denoted by $\mathcal{V}^\emptyset = (E, F, V, \emptyset)$.

The definition as such is abstract and can be instantiated by concrete implementations of processes and functions. For instance, the following combined loss function (Eq. 1) generalizes loss functions adopted by both the feature-based and trigger-set based watermarking methods:

$$L = L_c(f(\mathbf{W}, \mathbf{X}_r), \mathbf{y}_r) + \lambda^t L_c(f(\mathbf{W}, \mathbf{X}_T), \mathbf{y}_T) + \lambda^r R(\mathbf{W}, s), \quad (1)$$

in which λ^t, λ^r are the relative weight hyper-parameters, $f(\mathbf{W}, \mathbf{X}_\cdot)$ are the network predictions with inputs \mathbf{X}_r or \mathbf{X}_T . L_c is the loss function like *cross-entropy* that penalizes discrepancies between the predictions and the target labels \mathbf{y}_r or \mathbf{y}_T . Signature $s = \{\mathbf{P}, \mathbf{B}\}$ consists of passports \mathbf{P} and signature string \mathbf{B} . The regularization terms could be either $R = L_c(\sigma(\mathbf{W}, \mathbf{P}), \mathbf{B})$ as in [1] or $R = \text{MSE}(\mathbf{B} - \mathbf{P}\mathbf{W})$ as in [3].

It must be noted that, for those DNN models that will be used for classification tasks, their inference performance $\mathcal{M}(\mathbb{N}[\mathbf{W}, \cdot, \cdot], \mathbf{D}_t) = L_c(f(\mathbf{W}, \mathbf{X}_t), \mathbf{y}_t)$ tested against a dataset $\mathbf{D}_t = \{\mathbf{X}_t, \mathbf{y}_t\}$ is independent of either the embedded signature s or trigger set \mathbf{T} . It is this independence that induces an invertible process for existing watermark-based methods as described next.

Proposition 1 (*Invertible process*). For a DNN ownership verification scheme \mathcal{V} as in Definition 1, if the fidelity process $F(\cdot)$ is independent of either the signature s or trigger set

\mathbf{T} , then there always exists an invertible process $I(\cdot)$ i.e. the scheme is invertible $\mathcal{V}^I = (E, F, V, I \neq \emptyset)$.

Proof. for a trained network $\mathbb{N}[\hat{\mathbf{W}}, \mathbf{T}, s]$ with signature s and/or trigger set \mathbf{T} embedded, the invert process $I(\cdot)$ can be constructed with the following steps:

- maintain the optimal weights $\hat{\mathbf{W}}$ unchanged;
- minimize the detection error (see III in Definition (1) in the main paper):
 - forge the *feature-based* watermarks $s' = \{\mathbf{P}', \mathbf{B}'\}$ by minimizing the distance $\{\mathbf{P}', \mathbf{B}'\} = \arg \min_{\mathbf{P}, \mathbf{B}} D_f(f_e(\hat{\mathbf{W}}, \mathbf{P}), \mathbf{B})$. *Remark:* attackers have to take $\mathbf{B}' \neq \mathbf{B}$, and in case that the watermark signature \mathbf{B} is unknown, attackers may assign random signature \mathbf{B}' , whose the probability of collision $\mathbf{B}' = \mathbf{B}$ is then exponentially low.
 - forge the trigger set $\mathbf{T}' = \{\mathbf{X}'_T, \mathbf{y}'_T\}$ by minimizing the (cross-entropy) loss $\{\mathbf{X}'_T, \mathbf{y}'_T\} = \arg \min_{\mathbf{X}_T, \mathbf{y}_T} L_c(f(\hat{\mathbf{W}}, \mathbf{X}_T), \mathbf{y}_T)$ between the prediction and the target labels.

3) fidelity evaluation is fulfilled since it is independent to both the forged signatures and trigger set, thus remain unchanged.

Remark: during the minimization of detection error, there is *no need of training data* which is not used in step 2 at all;

Remark: during the minimization of detection error, the *computational cost is minor* since the dimensionality of the optimization parameters i.e. $\{\mathbf{P}', \mathbf{B}'\}$ or $\mathbf{X}'_T, \mathbf{y}'_T$ is order of magnitude smaller, as compared to the number of DNN weights $\hat{\mathbf{W}}$. \square

B. Watermark-based DNN in the face of ambiguity attacks

In this section, we investigate a number of watermark-based DNN ownership verification methods in the face of ambiguity attacks, which aim to cast doubts on ownership verification by forging counterfeit watermarks.

1) *Ambiguity attacks on feature-based method [1]:* Herein, we first train a DNN model embedded with watermarks as described in [1], then we conduct the ambiguity attacks as follows. The loss function adopted in [1] uses the following binary cross entropy for the embedding regularizer:

$$E_R(W) = - \sum_{j=1}^T (b_j \log(y_j) + (1 - b_j) \log(1 - y_j)), \quad (2)$$

in which $y_j = \sigma(\sum_i X_{ji} w_i)$ is the extracted feature with $\sigma(\cdot)$ is the sigmoid function. In order to forge watermark X for a given signature b_j , we first freeze the weights w_i of the watermarked DNN model, and minimize the loss (Eq. 2) with respect to the new binary signatures b'_j .

Fig. 2a illustrates the distributions of counterfeit watermarks X_{ji} together with the original watermarks, which are hardly distinguishable from each other. In terms of the extracted features $\sum_i X_{ji} w_i$, their distributions are different from the original watermarks, but it is still impossible to tell the difference between them after thresholding for the purpose of ownership verification. Finally, Fig. 2c illustrates that the

	Feature based method [1]			Trigger-set based method [2]		
	CIFAR10	Real WM Det.	Fake WM Det.	CIFAR10	Real WM Det.	Fake WM Det.
CIFAR100	64.25 (90.97)	100 (100)	100 (100)	65.20 (91.03)	25.00 (100)	27.80 (100)
Caltech-101	74.08 (90.97)	100 (100)	100 (100)	75.06 (91.03)	43.60 (100)	46.80 (100)

TABLE I: Detection of embedded watermark (in %) with two representative watermark-based DNN methods [1], [2], before and after DNN weights fine-tuning for transfer learning tasks. Top row denotes a DNN model trained with CIFAR10 and weights fine-tuned for CIFAR100; while bottom row denotes weight fine-tuned for Caltech-101. Accuracy outside bracket is the transferred task, while in-bracket is the original task. WM Det. denotes the detection accuracies of real and fake watermarks.

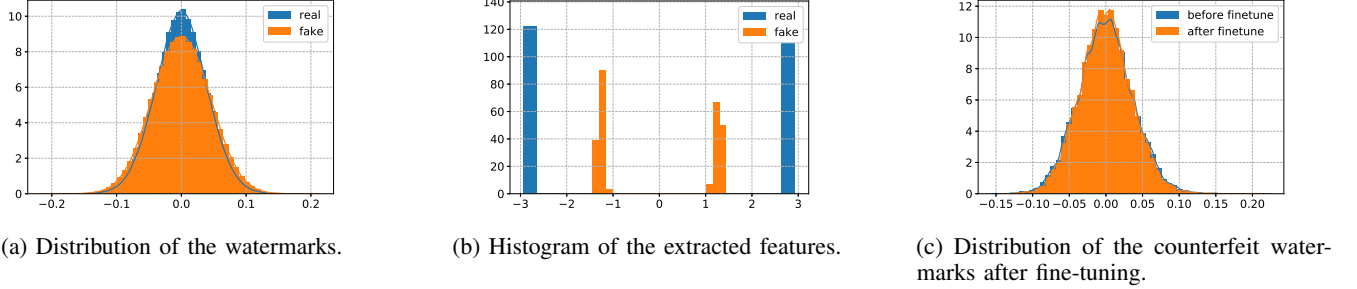


Fig. 2: A comparison of the distributions of watermarks and extracted features.

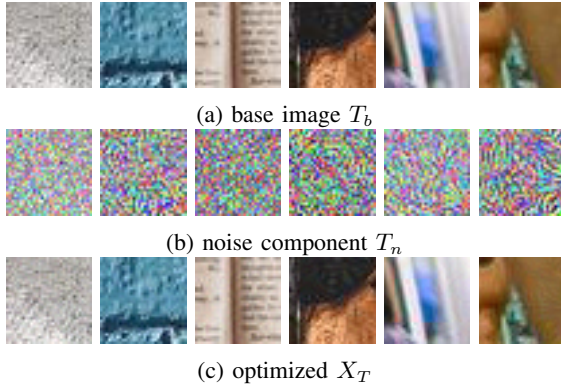


Fig. 3: Sample of the trigger set images used in ambiguity attacks on trigger-set based method in Section II-B2.

distribution of X_{ji} is not much affected by the fine-tuning process which aims to modify the DNN weights for transfer learning purposes (see Table I).

Following [1], we detect watermarks by comparing the extracted binary strings w.r.t. the designated one by measuring the successful detection rate. As summarized in Table I, all the counterfeit watermarks of size (256-bit) are successfully detected. We also fine-tune the DNN model by adjusting the network weights at all layers for new classification tasks (i.e. CIFAR100 and Caltech-101), where counterfeit watermarks are still detectable with 100% detection rate, demonstrating robustness against fine-tuning too.

Note that since w_i are fixed, we do not need to include the original (cross-entropy) loss measured with the training images, which is a constant during the optimization. This simplicity allows the forging of X_{ji} converge very rapidly. Note that, the overall optimization took about only 50 iterations in 50 seconds, which merely constitutes a minor fraction (2.5%) of the training time for the original task.

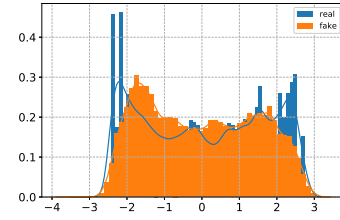


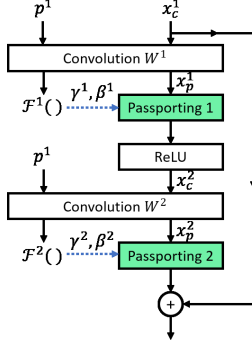
Fig. 4: Distribution of the real T_b and fake X_T trigger set images. It shows that the fake trigger set images are hardly distinguishable from the real ones.

2) *Ambiguity attacks on trigger-set based method [2]:* We first follow [2] to train the DNN model with trigger set images embedded as watermarks, and then we conduct the ambiguity attacks as follows. In order to construct the adversarial trigger set images by minimizing the cross-entropy loss between the predicted labels and the target labels, we adopt a simple approach which adds trainable noise components to randomly selected base images using the following steps:

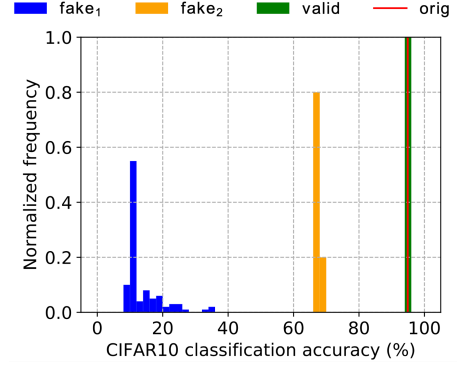
- 1) Randomly select a set of N base images T_b as shown in Fig. 3a;
- 2) Make random noisy patterns of the same size T_n as trainable parameters;
- 3) Use the summed components $\mathbf{X}_T = T_b + \eta T_n$ as the trigger set images, in which $\eta = 0.04$ to make the noise component invisible;
- 4) Randomly assign trigger set labels \mathbf{y}_T ;
- 5) Minimize the cross-entropy cost $L_c(f(\hat{\mathbf{W}}, \mathbf{X}_T), \mathbf{y}_T)$ w.r.t. the trainable parameter T_n .

Remark: DNN parameters $\hat{\mathbf{W}}$ are fixed during the optimization, and thus, the original training data is not needed.

Fig. 3c illustrates the final optimized \mathbf{X}_T , where all of them are correctly classified as the assigned labels i.e. \mathbf{y}_T . Visually, these forged trigger set images (Fig. 3c) are hardly



(a) An example in the *ResNet* layer that consists of the proposed passporting layers. $p^l = \{p_\gamma^l, p_\beta^l\}$ is the proposed *digital passports* where $\mathcal{F} = \text{Avg}(\mathbf{W}_p^l * \mathbf{P}_{\gamma, \beta}^l)$ is a passport function to compute the hidden parameters (i.e. γ and β) given in Eq. (3).



(b) A comparison of CIFAR10 classification accuracies given the original DNN, proposed DNN with valid passports, proposed DNN with randomly generated passports (*fake*₁), and proposed DNN with reverse-engineered passports (*fake*₂).

Fig. 5: (a) Passport layers in *ResNet* architecture and (b) Classification accuracies modulated by different passports in CIFAR10, e.g. given counterfeit passports, the DNN models performance will be deteriorated instantaneously to fend off illegal usage.

distinguishable from the original ones (Fig. 3a). In terms of histogram distributions, they are indistinguishable too (see Fig. 4). As shown in Table I, both the trigger set and forged images are 100% correctly labeled with assigned adversarial labels. This indistinguishable situation casts doubt on ownership verification by trigger set images alone.

After fine-tuned to other classification tasks, however, the classification accuracies of both trigger set and forged images deteriorated drastically yet the detection rate of forged images is slightly better than that of the original trigger set images. We ascribed this improvement to the ambiguity attack procedures outlined above. In terms of the computational cost, the overall optimization requires only about 100 epochs of fake trigger set in 100 seconds, which merely constitutes a minor fraction (5%) of the training time for the original task.

3) *Summary on ambiguity attacks on watermark-based DNN*: As proved by Proposition 1, one is able to construct forged watermarks for any already watermarked networks. We tested the performances of two representative DNN watermarking methods [1], [2], and Table I shows that counterfeit watermarks can be forged for the given DNN models with 100% detection rate, and 100% fake trigger set images can be reconstructed as well in the original task. Given that the detection accuracies for the forged trigger set is slightly better than the original trigger set after fine-tuning, the claim of the ownership is ambiguous and cannot be resolved by neither feature-based nor trigger-set based watermarking methods. Shockingly, the computational cost to forge counterfeit watermarks is minor, and worst still this is achieved without the need of original training data.

As a whole, the ambiguity attacks against DNN watermarking methods are effective with minor computational and without the need of original training datasets. We ascribe this loophole to the crux that the loss of the original task i.e. $L_c(f(\tilde{\mathbf{W}}, \mathbf{X}_r), \mathbf{y}_r)$ is *independent* of the forged watermarks. In the next section, we shall illustrate a solution to defeat the ambiguity attacks.

III. EMBEDDING PASSPORTS FOR DNN OWNERSHIP VERIFICATION

The main motivation of embedding digital passports is to design and train DNN models in a way such that, their inference performances of the original task (i.e. classification accuracy) will be significantly *deteriorated due to the forged signatures*. We shall illustrate next first how to implement the desired property by incorporating the so called *passport layers*, followed by different ownership protection schemes that exploit the embedded passports to effectively defeat ambiguity attacks.

A. Passport layers

In order to control the DNN model functionalities by the embedded digital signatures i.e. *passports*, we proposed to append after a convolution layer a *passport layer*, whose scale factor γ and bias shift term β are dependent on both the convolution kernels \mathbf{W}_p and the designated passport \mathbf{P} as follows:

$$\mathbf{O}^l(\mathbf{X}_p) = \gamma^l \mathbf{X}_p^l + \beta^l = \gamma^l (\mathbf{W}_p^l * \mathbf{X}_c^l) + \beta^l, \quad (3)$$

$$\gamma^l = \text{Avg}(\mathbf{W}_p^l * \mathbf{P}_\gamma^l), \quad \beta^l = \text{Avg}(\mathbf{W}_p^l * \mathbf{P}_\beta^l), \quad (4)$$

in which $*$ denotes the convolution operations, l is the layer number, \mathbf{X}_p is the input to the passport layer and \mathbf{X}_c is the input to the convolution layer. $\mathbf{O}()$ is the corresponding linear transformation of outputs, while \mathbf{P}_γ^l and \mathbf{P}_β^l are the passports used to derive scale factor and bias term respectively. Figure 5a delineates the architecture of digital passport layers used in a *ResNet* layer.

Remark: for DNN models trained with passport $\mathbf{s}_e = \{\mathbf{P}_\gamma^l, \mathbf{P}_\beta^l\}^l$, their *inference performances* $\mathcal{M}(\mathcal{N}[\mathbf{W}, \mathbf{s}_e], \mathbf{D}_t, \mathbf{s}_t)$ depend on the running time passports \mathbf{s}_t i.e.

$$\mathcal{M}(\mathcal{N}[\mathbf{W}, \mathbf{s}_e], \mathbf{D}_t, \mathbf{s}_t) = \begin{cases} \mathcal{M}_{\mathbf{s}_e}, & \text{if } \mathbf{s}_t = \mathbf{s}_e, \\ \mathcal{M}_{\mathbf{s}_e}, & \text{otherwise.} \end{cases} \quad (5)$$

If the genuine passport is not presented $\mathbf{s}_t \neq \mathbf{s}_e$, the running time performance $\mathcal{M}_{\mathbf{s}_e}$ is significantly deteriorated because the

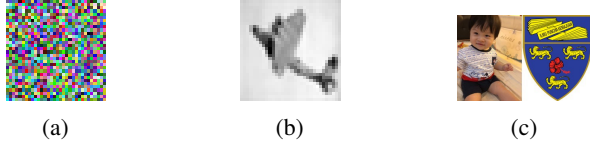


Fig. 6: Example of different types of passports: (a) random patterns, (b) fixed image and (c) random shuffled.

corresponding scale factor γ and bias terms β are calculated based on the wrong passports. For instance, as shown in Figure 5b, a proposed DNN model presented with valid passports (green) will demonstrate almost identical accuracies as to the original DNN model (red). In contrast, the same proposed DNN model presented with counterfeit passports (blue), the accuracy will deteriorate to merely about 10% only.

Remark: the gist of the proposed passport layer is to enforce *dependence* between scale factor, bias terms and network weights. As shown by the Proposition 2, it is this dependence that validates the required non-invertibility to defeat ambiguity.

Proposition 2 (Non-invertible process). A DNN ownership verification scheme \mathcal{V} as in Definition 1 is *non-invertible*, if

- I) the fidelity process outcome $F(\mathbb{N}[\mathbf{W}, \mathbf{T}, \mathbf{s}], \mathbf{D}_t, \mathcal{M}_t, \epsilon_f)$ depends either on the presented signature \mathbf{s} or trigger set \mathbf{T} ,
- II) with forged passport $\mathbf{s}_t \neq \mathbf{s}_e$, the DNN inference performance $\mathcal{M}(\mathbb{N}[\mathbf{W}, \mathbf{s}_e], \mathbf{D}_t, \mathbf{s}_t)$ in (Eq. 5) will deteriorate such that the discrepancy is larger than a threshold i.e. $|\mathcal{M}_{\mathbf{s}_e} - \overline{\mathcal{M}}_{\mathbf{s}_e}| > \epsilon_f$.

Proof. Since using forged passports the DNN model performance is significantly deteriorated such that $|\mathcal{M}_{\mathbf{P}_e} - \overline{\mathcal{M}}_{\mathbf{P}_e}| > \epsilon_f$, it immediately follows, from the definition of invertible verification schemes, that the scheme in question is non-invertible. \square

B. Methods to generate passports

Public parameters of a passport protected DNN might be easily plagiarized, then the plagiarizer has to deceive the network with certain passports. The chance of success of such an attacking strategy depends on the odds of correctly guessing the secret passports. Figure 6 illustrates three different types of passports which have been investigated in our work:

- a) *random patterns*, whose elements are independently randomly generated according to the uniform distribution between $[-1, 1]$.
- b) one selected image is fed through a trained DNN model with the same architecture, and the corresponding feature maps are collected. Then the selected *image* is used at the input layer and the *corresponding feature* maps are used at other layers as passports. We refer to passports generated as such the *fixed image* passport.
- c) a set of N selected *images* are fed to a trained DNN model with the same architecture, and N corresponding *feature maps* are collected at each layer. Among the N options, only one is randomly selected as the passport at each



Fig. 7: Randomly shuffled passports in a 5-layered passport AlexNet_P. From left to right: Conv1 to Conv5 layers where the 4 passports in Conv2 to Conv5 corresponding to the first 4 channel of each layer.

layer. Specifically, for a set of N images being applied to a DNN model with L layers, there are altogether N^L possible combinations of passports that can be generated. We refer to passports generated as such the *randomly shuffled* image passports.

Since randomly shuffled passports allow strong protection and flexibility in the passport generation and distribution, we adopt this passport generation method for all the experiments reported in this paper. Specifically, 20 images are selected and fed to the DNN architectures that are used in our experiments. Passports at those corresponding convolution layers are then collected as possible passports. Some example of the features maps selected as the passports at different layers are illustrated in Figure 7.

C. Sign of scale factors as signature

During learning the DNN, to further protect the DNN models ownership from insider threat (e.g. a former staff who establish a new start-up business with all the resources stolen from originator), one can enforce the scale factor γ to take either positive or negative signs (+/-) as designated, so that it will form a unique signature string (like fingerprint). This process is done by adding the following *sign loss* regularization term into the combined loss (Eq. 1):

$$R(\gamma, \mathbf{P}, \mathbf{B}) = \sum_{i=1}^C \max(\gamma_0 - \gamma_i b_i, 0) \quad (6)$$

in which $\mathbf{B} = \{b_1, \dots, b_C\} \in \{-1, 1\}^C$ consists of the designated binary bits for C convolution kernels, and γ_0 is a positive control parameter (0.1 by default unless stated otherwise) to encourage the scale factors have magnitudes greater than γ_0 .

It must be highlighted that the inclusion of sign loss (Eq. 6) enforces the scale factors γ to take either positive or negative values, and the signs enforced in this way remain rather persistent against various adversarial attacks. This feature explains the superior robustness of embedded passports against ambiguity attacks by reverse-engineering shown in Sect. IV-D.

D. Ownership verification with passports

Taking advantages of the proposed passport embedding method, we design three ownership verification schemes that are summarized in Fig. 8. We briefly introduce them next and their respective merits and demerits, in terms of computational complexity, ease to use and protection strengths etc. are summarized in Table II. Note that, in order to enhance the

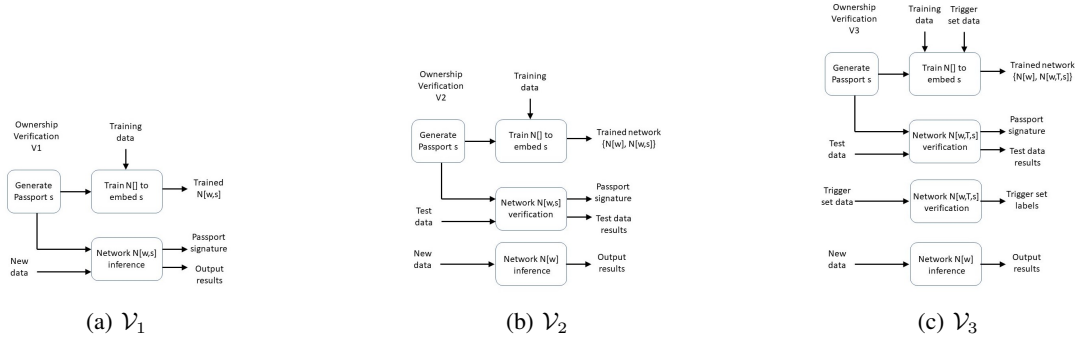


Fig. 8: A graphical comparison of three different ownership verification schemes \mathcal{V} with passports.

Algorithm 1 Forward pass of a passport layer using scheme \mathcal{V}_1

- 1: **procedure** FORWARD $\mathcal{V}_1(X_c, W_p, P_\gamma, P_\beta)$
 - 2: $\gamma \leftarrow \text{Avg}(W_p * P_\gamma)$
 - 3: $\beta \leftarrow \text{Avg}(W_p * P_\beta)$
 - 4: $X_p \leftarrow W_p * X_c$
 - 5: $Y_p \leftarrow \gamma * O(X_p) + \beta \triangleright O$ is a linear transformation such as BatchNorm
 - 6: **return** Y_p
-

justification of ownership, one can furthermore select either personal identification pictures or corporate logos (Figure 6c) during the designing of the fixed or random image passports. Also, it must be noted that, using passports as proofs of ownership to stop infringements is the last resort, only if the hidden parameters are illegally disclosed or (partially) recovered. We believe this juridical protection is often not necessary since the proposed technological solution actually provides proactive, rather than reactive, IP protection of deep neural networks.

\mathcal{V}_1 : Passport is distributed with the trained DNN model

Hereby, the *learning* process aims to minimize the combined loss function (Eq. 1), in which $\lambda_t = 0$ since trigger set images are not used in this scheme and the sign loss (Eq. 6) is added as the regularization term. The trained DNN model together with the passport are then distributed to legitimate users, who perform network *inferences* with the given *passport* fed to the passport layers as shown in Figure 5a. The network ownership is automatically verified by the distributed passports. As shown by Table VI and Figure 11, this ownership verification is robust to DNN model modifications. Also, as shown in Figure 5, ambiguity attacks are not able to forge a set of passport and signature that can maintain the DNN inference performance.

The downside of this scheme is the requirement to use passports during inferencing, which leads to extra computational cost by about 10% (see Sect. IV-F). Also the distribution of passports to the end-users is intrusive and imposes additional responsibility of guarding the passports safely.

\mathcal{V}_2 : Private passport is embedded but not distributed

Herein, the *learning* process aims to simultaneously achieve *two goals*, of which the first is to minimize the original task loss (e.g. classification accuracy discrepancy) when *no*

Algorithm 2 Training step for scheme \mathcal{V}_1

- 1: initialize a passport model M_s with desired number of passport layers, N_{pass}
 - 2: initialize passport keys P in M_s
 - 3: encode desired *signature* s into binary to be embedded into signs of γ_p of all passport layers
 - 4: **for** number of training iterations **do**
 - 5: sample minibatch of m samples $X \{X^{(1)}, \dots, X^{(m)}\}$ and targets $Y \{Y^{(1)}, \dots, Y^{(m)}\}$
 - 6: **if** enable backdoor **then**
 - 7: sample t samples of T and backdoor targets $Y_T \triangleright t = 2$, default by [2]
 - 8: concatenate X with T , Y with Y_T
 - 9: compute cross-entropy loss L_c using X and Y
 - 10: **for** l in N_{pass} **do**
 - 11: compute sign loss R^l using s^l and γ_p^l
 - 12: $R \leftarrow \sum_l^{N_{pass}} R^l$
 - 13: compute combined loss L using L_c and R
 - 14: backpropagate using L and update M_p
-

passport layers included; and the second is to minimize the combined loss function (Eq. 1) with passports regularization included. Algorithm-wise, this *multi-task learning* is achieved by alternating between the minimization of these two goals. The successfully trained DNN model is then distributed to end-users, who may perform network inference *without the need of passports*. Note that this is possible since passport layers are not included in the distributed networks. The ownership verification will be carried out only upon requested by the law enforcement, by adding the passport layers to the network in question and detecting the embedded sign signatures with unyielding the original network inference performances.

Compared with scheme \mathcal{V}_1 , this scheme is easy to use for end-users since no passport is needed and no extra computational cost is incurred. In the meantime, this ownership verification is robust to removal attacks as well as ambiguity attacks. The downside, however, is the requirement to access the DNN weights and to append the passport layers for ownership verification, i.e. the disadvantages of white-box protection mode as discussed in [2]. Therefore, we propose to combine it with trigger-set based verification that will be described next.

\mathcal{V}_3 : Both the private passport and trigger set are

	Passport used	Trigger set used for verification	Weights needed for verification	Multi-task Learning	E	M for F	V
\mathcal{V}_1	$\begin{cases} \text{Yes,} & \text{inf.} \\ \text{Yes,} & \text{verif.} \end{cases}$	No	Yes	No	$\mathcal{N}[\mathbf{W}, \mathbf{s}_e]$	$\begin{cases} \mathcal{M}_{\mathbf{s}_e}, & \text{if } \mathbf{s}_t = \mathbf{s}_e, \\ \mathcal{M}_{\mathbf{s}_e}, & \text{otherwise.} \end{cases}$	$V(\mathcal{N}[\mathbf{W}, \mathbf{s}_e])$
\mathcal{V}_2	$\begin{cases} \text{No,} & \text{inf.} \\ \text{Yes,} & \text{verif.} \end{cases}$	No	Yes	Yes	$\begin{cases} \mathcal{N}[\mathbf{W}], & \text{inf.} \\ \mathcal{N}[\mathbf{W}, \mathbf{s}_e], & \text{verif.} \end{cases}$	$\begin{cases} \mathcal{M}_{\mathbf{s}_e}, & \text{inf.} \\ \mathcal{M}_{\mathbf{s}_e}, & \text{if } \mathbf{s}_t = \mathbf{s}_e, \\ \mathcal{M}_{\mathbf{s}_e}, & \text{otherwise.} \end{cases}$	$\begin{cases} \text{Not needed,} & \text{inf.} \\ V(\mathcal{N}[\mathbf{W}, \mathbf{s}_e]), & \text{verif.} \end{cases}$
\mathcal{V}_3	$\begin{cases} \text{No,} & \text{inf.} \\ \text{Yes,} & \text{verif.} \end{cases}$	Yes	$\begin{cases} \text{No,} & \text{verif.T,} \\ \text{Yes,} & \text{verif.P} \end{cases}$	Yes	$\begin{cases} \mathcal{N}[\mathbf{W}], & \text{inf.} \\ \mathcal{N}[\mathbf{W}, \mathbf{T}, \mathbf{s}_e], & \text{verif.} \end{cases}$	$\begin{cases} \mathcal{M}_{\mathbf{s}_e}, & \text{inf.} \\ \mathcal{M}_{\mathbf{s}_e}, & \text{if } \mathbf{s}_t = \mathbf{s}_e, \\ \mathcal{M}_{\mathbf{s}_e}, & \text{otherwise.} \end{cases}$	$\begin{cases} \text{Not needed,} & \text{inf.} \\ V(\mathcal{N}[\mathbf{W}, \mathbf{T}, \mathbf{s}_e]), & \text{verif.T} \\ V(\mathcal{N}[\mathbf{W}, \mathbf{s}_e]), & \text{verif.P} \end{cases}$

TABLE II: A comparison of the features of the three passport-based ownership verification schemes depicted in Section III-D. See Definition (1) for process E, F, V and Eq. (5) for the proposed DNN model performances M . Notations: "inf." is network inference; "verif" is ownership verification; "verif.P" is verification by passport (white-box); "verif.T" is by trigger set samples (black-box).

Algorithm 3 Forward pass of a passport layer using scheme \mathcal{V}_2 and \mathcal{V}_3

```

1: procedure FORWARD  $\mathcal{V}_{23}(X_c, W_p, P_\gamma, P_\beta, \gamma_{\text{publ}}, \beta_{\text{publ}}, \text{idx})$ 
2:   if  $\text{idx} = 0$  then
3:      $X_p \leftarrow W_p * X_c$ 
4:      $Y_p \leftarrow \gamma_{\text{publ}} * O(X_p) + \beta_{\text{publ}} \triangleright \gamma_{\text{publ}}$  and  $\beta_{\text{publ}}$  is a public parameter
5:   return  $Y_p$ 
6:   else
7:   return FORWARD  $\mathcal{V}_1(X_c, W_p, P_\gamma, P_\beta)$ 

```

Algorithm 4 Sign Loss

```

1: procedure SIGN LOSS( $B^l, W_p^l, P_\gamma^l, \gamma_0$ )
2:    $\gamma^l \leftarrow \text{Avg}(W_p^* P_\gamma^l)$ 
3:    $\text{loss} \leftarrow \max(\gamma_0 - \gamma^l * B^l, 0) \triangleright \gamma_0$  is a positive constant, equals 0.1 as by default
4:   return loss

```

embedded but not distributed

This scheme only differs from scheme \mathcal{V}_2 in that, a set of trigger images is embedded in addition to the embedded passports. The advantage of this, as discussed in [2] is to probe and claim ownership of the suspect DNN model through remote calls of service APIs. This capability allows one, first to claim the ownership in a black-box mode, followed by reassertion of ownership with passport verification in a white box mode. Algorithm-wise, the embedding of trigger set images is jointly achieved in the same minimization process that embeds passports in scheme \mathcal{V}_2 . Finally, it must be noted that the embedding of passports in both \mathcal{V}_2 and \mathcal{V}_3 schemes are implemented through *multi-task learning tasks* where we adopted group normalisation [11] instead of batch normalisation [12] that is not applicable due to its dependency on running average of batch-wise training samples.

1) *Algorithms*: Pseudo-code of the three verification schemes are illustrated in this section. For reproducibility of this work, we will make publicly available all source codes as well as the training / test datasets that are used in this paper, together with the camera-ready of the submission should the manuscript be accepted.

Using Algorithm 5, we can extract a binarized version of

Algorithm 5 Signature detection

```

1: procedure SIGNATURE DETECTION( $W_p, P_\gamma$ )
2:    $\gamma \leftarrow \text{Avg}(W_p * P_\gamma)$ 
3:    $\text{signature} \leftarrow \text{sign}(\gamma)$ 
4:   convert  $\text{signature}$  into binary
5:   decode binarized  $\text{signature}$  into desired format e.g. ascii
6:   match decoded  $\text{signature}$  with target signature

```

signature s where positive γ is 1 and negative γ is 0 from model M_p . We can then decode s into desired format such as ASCII code. Finally, we can claim ownership of the model M_p .

2) *Multi-task learning with private passports and/or trigger set images*: The multi-task learning algorithms used for embedding passports in schemes \mathcal{V}_2 and \mathcal{V}_3 are summarized in Algorithm 6 which is similar to Algorithm 2.

It must be noted that the practical choice of formula (Eq. 3) is inspired by the well-known *Batch Normalization* (BN) layer which essentially applies the channel-wise linear transformation to the inputs². Nevertheless BN is not applicable to multi-task learning tasks because of its dependency on running average of batch-wise training samples. When BN is used for multi-task learning, the test accuracy is significantly reduced even though the training accuracy seems optimized. We therefore adopted *group normalization* (GN) in the baseline DNN model for schemes \mathcal{V}_2 and \mathcal{V}_3 reported in Table VI³.

IV. EXPERIMENT RESULTS

This section illustrates the empirical study of passport-based DNN models, with focuses on *convergence* and *effectiveness* of passport layers. Whereas the inference performances of various schemes are also compared in terms of *robustness* to both removal attacks and ambiguity attacks. The network architectures we investigated include the well-known AlexNet and ResNet-18 and in order to avoid confusion to the original AlexNet and ResNet models, we denote AlexNet_p and ResNet_p-18 as our proposed passport-based DNN models. Table III-IV show the detailed architecture and hyper-parameters for both

²Sergey Ioffe, Christian Szegedy, "Batch Normalization: Accelerating Deep Network Training by Reducing Internal Covariate Shift", ICML2015, pp. 448-456.

³Yuxin Wu, Kaiming He, "Group Normalization", ECCV2018, pp. 3-19.

Algorithm 6 Training step for scheme \mathcal{V}_2 and \mathcal{V}_3

```

1: initialize a passport model  $M_s$  with desired number of
  passport layers,  $N_{pass}$ 
2: if enable trigger set then ▷ for scheme  $\mathcal{V}_3$ 
3:   initialize trigger sets  $T$ 
4:   initialize passport keys  $P$  in  $M_s$  using  $T$ 
5: else
6:   initialize passport keys  $P$  in  $M_s$ 
7: encode desired signature  $s$  into binary to be embedded
  into signs of  $\gamma_p$  of all passport layers
8: for number of training iterations do
9:   sample minibatch of  $m$  samples  $X \{X^{(1)}, \dots, X^{(m)}\}$ 
  and targets  $Y \{Y^{(1)}, \dots, Y^{(m)}\}$ 
10:  if enable backdoor then
11:    sample  $t$  samples of  $T$  and backdoor targets  $Y_T$  ▷
     $t = 2$ , default by [2]
12:    concatenate  $X$  with  $T$ ,  $Y$  with  $Y_T$ 
13:    for  $idx$  in  $0 \ 1$  do
14:      if  $idx = 0$  then
15:        compute cross-entropy loss  $L_c$  using  $X$ ,  $Y$  and
         $\gamma_{publ}$ 
16:      else
17:        compute cross-entropy loss  $L_c$  using  $X$  and  $Y$ 
18:        for  $l$  in  $N_{pass}$  do
19:          compute sign loss  $R^l$  using  $s^l$  and  $\gamma_p^l$ 
20:         $R \leftarrow \sum_l^{N_{pass}} R^l$ 
21:        compute combined loss  $L$  using  $L_c$  and  $R$ 
22:        backpropagate using  $L$  and update  $M_p$ 

```

AlexNet_p and ResNet_p-18 that employed in all the experiments, unless stated wise. Two publicly datasets - CIFAR10 and CIFAR100 classification tasks are employed because these medium-sized public datasets allow us to perform extensive tests of the DNN model performances. Unless stated otherwise, all experiments are repeated 5 times and tested against 50 fake passports to get the mean inference performance.

A. Convergence

The introduction of the proposed passport layers does not hinder the convergence of DNN learning process. As shown in Figure 9, we observe that the test accuracies converge in synchronization with the network weights, and computed linear transformation parameters γ and β which all stagnate in the later learning phase when the learning rate is reduced from 0.01 to 0.0001.

B. Effectiveness

With the introduction of the passport layers, we essentially separate the DNN parameters into two types: the *public* convolution layer parameters \mathbf{W} and the *hidden*⁴ passport layer - i.e. scale factor γ and bias terms β (see Eq. (5)). The learning of each of these parameter types are different too. On one

hand, the distribution of the convolution layer weights seems identical to that of the original DNN without passport layers (Figure 10a). However, we must emphasize that information about the passports are embedded into weights \mathbf{W} in the sense that following constraints are enforced once the learning is done:

$$\text{Avg}(\mathbf{W}_p^l * \mathbf{P}_\gamma^l) = c_\gamma^l, \quad \text{Avg}(\mathbf{W}_p^l * \mathbf{P}_\beta^l) = c_\beta^l, \quad (7)$$

where c_γ^l, c_β^l are two constants of converged parameters γ^l, β^l .

On the other hand, the distribution of the hidden parameters are affected by the adoption of sign loss (Eq. 6). Clearly the scale factors are enforced to take either positive or negative values far from zero (Figure 10b). We also observe that the sign of scale factors remain rather persistent against various adversarial attacks. An additional benefit of enforcing non-zero magnitudes of scale factors is to ensure the non-zero channel outputs and slightly improve the performances. Correspondingly the distribution of bias terms becomes more balanced with the sign loss regularization (Eq. 6) included, whereas the original bias terms are mainly negative valued (Figure 10c).

C. Robustness against removal attacks

1) *Fine-tuning*: In this experiment, we repeatedly trained each model five times with designated scale factor signs embedded into both AlexNet_p and ResNet_p-18 networks. Table VI shows that the passport signatures are detected at near to 100% accuracy for all the ownership verification schemes in the original task. Even after fine-tuning the proposed DNN models for a new task (e.g. from CIFAR10 to Caltech-101), almost 100% detection rates of the embedded passport are still maintained. Note that a detected signature is claimed only *iff* all the binary bits are exactly matched. We ascribe this superior robustness to the unique controlling nature of the scale factors — in case that a scale factor value is reduced near to zero, the channel output will be virtually zero, thus, its gradient will vanish and lose momentum to move towards to the opposite value. Empirically we have not observed counter-examples against this explanation⁵.

Table V shows the trigger set image detection rate before and after fine-tuning. Note that passports are not used in this experiment, therefore, the detection rate of the trigger set labels deteriorated drastically after fine-tuning. Nevertheless, trigger set images can still be used in scheme \mathcal{V}_3 to complement the white-box passport-based verification approach.

2) *Model pruning*: The aim of model pruning is to reduce redundant parameters without compromise the performance. Here, we adopt the *class-blind* pruning scheme in [14], and test our proposed DNN models with different pruning rates. Figure 11 shows that, in general, our proposed DNN models still maintained near to 100% accuracy even 60% parameters are pruned, while the accuracy of testing data drops around 5%-25%. Even if we prune 90% parameters, the accuracy of our proposed DNN models are still much higher than the accuracy of testing data. As said, we ascribe the robustness

⁴In this work, traditional hidden layer parameters are considered as public parameters.

⁵A rigorous proof of this argument is under investigation and will be reported elsewhere.

layer name	output size	weight shape	padding
Conv1	32×32	$64 \times 3 \times 5 \times 5$	2
MaxPool2d	16×16	2×2	
Conv2	16×16	$192 \times 64 \times 5 \times 5$	2
Maxpool2d	8×8	2×2	
Conv3	8×8	$384 \times 192 \times 3 \times 3$	1
Conv4	8×8	$256 \times 384 \times 3 \times 3$	1
Conv5	8×8	$256 \times 256 \times 3 \times 3$	1
MaxPool2d	4×4	2×2	
Linear	10	10×4096	

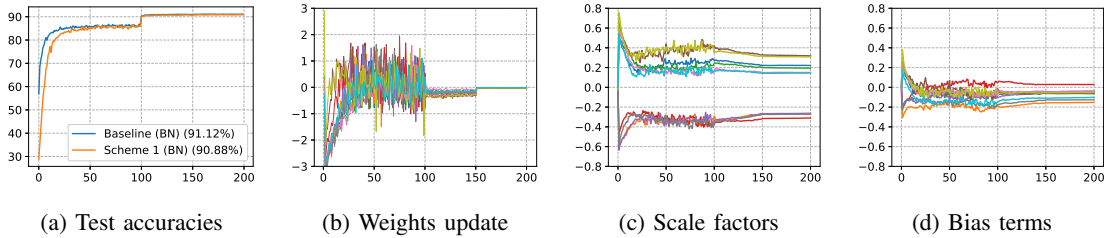
layer name	output size	weight shape	padding
Conv1	32×32	$64 \times 3 \times 3 \times 3$	1
Conv2_x	32×32	$\begin{matrix} 64 \times 64 \times 3 \times 3 \\ 64 \times 64 \times 3 \times 3 \end{matrix} \times 2$	1
Conv3_x	16×16	$\begin{matrix} 128 \times 128 \times 3 \times 3 \\ 128 \times 128 \times 3 \times 3 \end{matrix} \times 2$	1
Conv4_x	8×8	$\begin{matrix} 256 \times 256 \times 3 \times 3 \\ 256 \times 256 \times 3 \times 3 \end{matrix} \times 2$	1
Conv5_x	4×4	$\begin{matrix} 512 \times 512 \times 3 \times 3 \\ 512 \times 512 \times 3 \times 3 \end{matrix} \times 2$	1
Average pool	1×1	4×4	
Linear	10	10×512	

TABLE III: (Left:) AlexNet_p architecture. (Right): ResNet_p-18 architecture

Hyper-parameter	AlexNet _p	ResNet _p -18
Activation function	ReLU	ReLU
Optimization method	SGD	SGD
Momentum	0.9	0.9
Learning rate	0.01, 0.001, 0.0001†	0.01, 0.001, 0.0001†
Batch size	64	64
Epochs	200	200
Learning rate decay	0.001 at epoch 100 and 0.0001 at epoch 150	0.001 at epoch 100 and 0.0001 at epoch 150
Weight Initialization	[13]	[13]
Passport Layers	Conv3,4,5	Conv5_x

TABLE IV: Training parameters for AlexNet_p and ResNet_p-18, respectively († the learning rate is scheduled as 0.01, 0.001 and 0.0001 between epochs [1-100], [101-150] and [151-200] respectively).

	Trigger Set Detection	To CIFAR10	To CIFAR100	To Caltech-101
AlexNet CIFAR10	100%	-	24.67%	57.67%
AlexNet CIFAR100	100%	36.00%	-	78.67%
ResNet CIFAR10	100%	-	12.50%	13.67%
ResNet CIFAR100	100%	6.33%	-	4.67%

TABLE V: Detection rate of the trigger set images (before and after fine-tuning) used in scheme \mathcal{V}_3 to complement passport-based verifications.Fig. 9: (a) Convergences of test accuracies, (b) weight updates, (c) scale factors, and (d) bias terms of first 10 channels in Conv4 of AlexNet_p. x-axis: training epochs; y-axis: see captions of subfigures.

against model pruning to the superior persistence of signatures embedded in the scale factor signs (see Sect. III-C).

D. Resilience against ambiguity attacks

As shown in Fig. 12, the accuracy of our proposed DNN models trained on CIFAR10/100 classification task is significantly depending on the presence of either valid or counterfeit passports — the proposed DNN models presented with valid passports demonstrated almost identical accuracies as to the original DNN model. Contrary, the same proposed DNN model presented with invalid passports (in this case of $fake_1$ = random attack) achieved only 10% accuracy which is merely

equivalent to a random guessing. In the case of $fake_2$, we assume that the adversaries have access to the original training dataset, and attempt to reverse-engineer the scale factor and bias term by freezing the trained DNN weights. It is shown that in Fig. 12, reverse-engineering attacks are only able to achieve, for CIFAR10, at best 84% accuracy on AlexNet_p and 70% accuracy on ResNet_p-18. While in CIFAR100, for $fake_1$ case, attack on both our proposed DNN models achieved only 1% accuracy; for $fake_2$ case, this attack only able to achieve 44% accuracy for AlexNet_p and 35% accuracy for ResNet_p-18.

1) *Random attacks*: The following experiments aim to disclose the dependence of the original task performances with

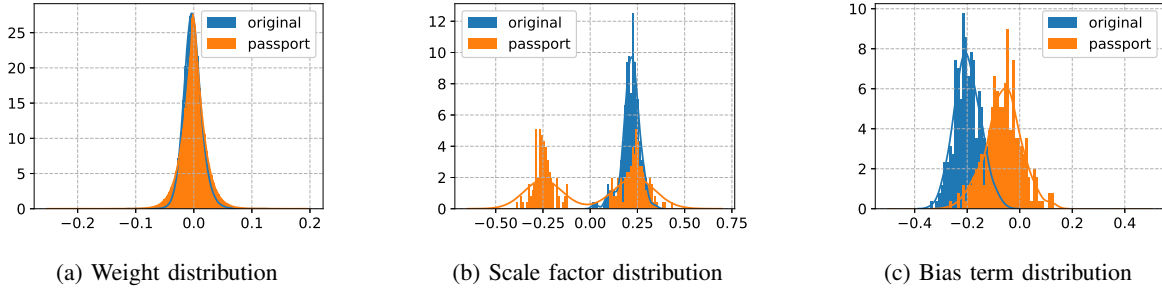


Fig. 10: Comparison of the distributions of (a) network weights, (b) scale factors, and (c) bias terms between the original and passport DNN (Conv4 of AlexNet_p)

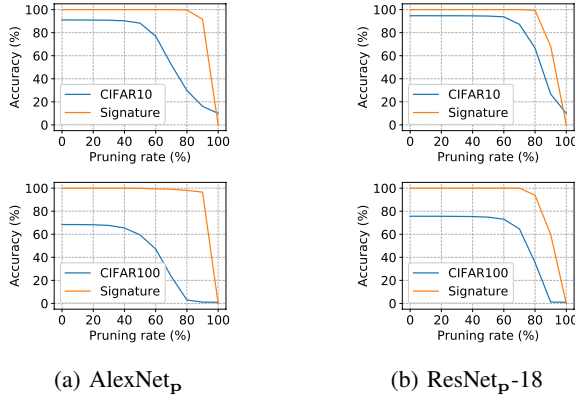


Fig. 11: Removal Attack (Model Pruning): Classification accuracy of our passport-based DNN models on both CIFAR10/CIFAR100 and signature detection accuracy against different pruning rates.

respect to the crucial parameter *scale factors*, and specifically, its positive/negative signs.

In the first experiment, for the passport-embedded DNN models, we simulate random attacks by flipping the signs of certain randomly selected scale factors and then measure the performance. It turns out that the final performance are sensitive to the change of signs — majority of the DNN model performances drop significantly as long as more than (at least) 50% of scale factors have flipped signs as shown in Figure 13 and Figure 14, respectively. The deteriorated performances are more pronounced when the passports are embedded in either all the three convolution layers (3-4-5) in AlexNet_p (right-most column in Figure 13) or the last blocks in ResNet_p-18 (Figure 14), whose performances drop to about 10% and 1% respectively.

The simulation results summarized in Figure 13 and Figure 14 are in accordance to the results illustrates in Figure 12, which shows that the performance of passport-embedded DNNs under the attack of randomly assigned passport signatures. The poor performances measured for both AlexNet_p and ResNet_p-18 on CIFAR10/CIFAR100 tasks are in the range of [10%, 30%] and [1%, 3%] respectively.

2) *Reversed-engineering attacks*: In this experiment, we further assume the adversaries have the access to original training data and thus are able to maximize the original

CIFAR10			
AlexNet _p	CIFAR10	CIFAR100	Caltech-101
Baseline (BN)	- (91.12)	- (65.53)	- (76.33)
Scheme \mathcal{V}_1	100 (90.91)	100 (64.64)	100 (73.03)
Baseline (GN)	- (90.88)	- (62.17)	- (73.28)
Scheme \mathcal{V}_2	100 (89.44)	99.91 (59.31)	100 (70.87)
Scheme \mathcal{V}_3	100 (89.15)	99.96 (59.41)	100 (71.37)
ResNet _p -18			
Baseline (BN)	- (94.85)	- (72.62)	- (78.98)
Scheme \mathcal{V}_1	100 (94.62)	100 (69.63)	100 (72.13)
Baseline (GN)	- (93.65)	- (69.40)	- (75.08)
Scheme \mathcal{V}_2	100 (93.41)	100 (63.84)	100 (71.07)
Scheme \mathcal{V}_3	100 (93.26)	99.98 (63.61)	99.99 (72.00)
CIFAR100			
AlexNet _p	CIFAR100	CIFAR10	Caltech-101
Baseline (BN)	- (68.26)	- (89.46)	- (79.66)
Scheme \mathcal{V}_1	100 (68.31)	100 (89.07)	100 (78.83)
Baseline (GN)	- (65.09)	- (88.30)	- (78.08)
Scheme \mathcal{V}_2	100 (64.09)	100 (87.47)	100 (76.31)
Scheme \mathcal{V}_3	100 (63.67)	100 (87.46)	100 (75.89)
ResNet _p -18			
Baseline (BN)	- (76.25)	- (93.22)	- (82.88)
Scheme \mathcal{V}_1	100 (75.52)	100 (95.28)	99.99 (79.27)
Baseline (GN)	- (72.06)	- (91.83)	- (79.15)
Scheme \mathcal{V}_2	100 (72.15)	100 (90.94)	100 (77.34)
Scheme \mathcal{V}_3	100 (72.10)	100 (91.30)	100 (77.46)

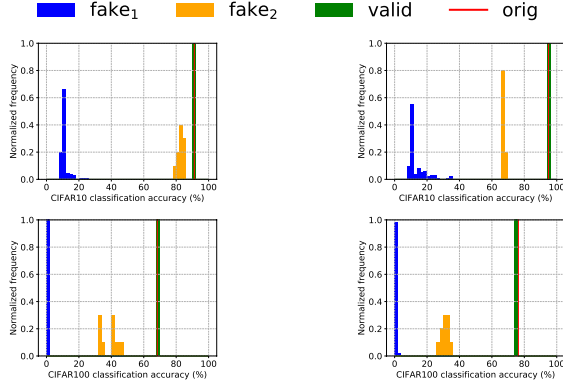
TABLE VI: Removal Attack (Fine-tuning): Detection/Classification accuracy (in %) of different passport networks where BN = batch normalisation and GN = group normalisation. (Left: trained with CIFAR10 and fine-tune for CIFAR100/Caltech-101. Right: trained with CIFAR100 and fine-tune for CIFAR10/Caltech-101.) Accuracy outside bracket is the signature detection rate, while in-bracket is the classification rate.

task performance by reverse-engineering scale factors (i.e. flipping the sign (+/-) of the scale factor). The trained AlexNet_p/ResNet_p-18 are used for this experiment, and it turns out the best performance the adversary can achieve is no more than 84%/70% for CIFAR10 and 40%/38% for CIFAR100 classifications respectively (see Figure 15).

Summary Extensive empirical studies show that it is impossible for adversaries to maintain the original DNN model

Ambiguity attack modes	Attackers have access to	Ambiguous passport construction methods	Invertibility (see Def. 1.V)	Verification scheme \mathcal{V}_1	Verification scheme \mathcal{V}_2	Verification scheme \mathcal{V}_3
$fake_1$	W	- Random passport P_r	- $F(P_r)$ fail, by large margin	Large accuracy \downarrow	Large accuracy \downarrow	Large accuracy \downarrow
$fake_2$	$W, \{D_r; D_t\}$	- Reverse engineer passport P_e	- $F(P_e)$ fail, by moderate margin	Moderate accuracy \downarrow	Moderate accuracy \downarrow	Moderate accuracy \downarrow
$fake_3$	$W, \{D_r; D_t\}, \{P, S\}$	- Reverse engineer passport $\{P_e; S_e\}$ by exploiting original passport P & sign string S	- if $S_e = S$: $F(P_e)$ pass, with negligible margin - if $S_e \neq S$: $F(P_e)$ fail, by moderate to huge margin	see Figure 16	see Figure 16	see Figure 16

TABLE VII: Summary of overall passport network performances in Scheme \mathcal{V}_1 , \mathcal{V}_2 and \mathcal{V}_3 , respectively under three different ambiguity attack modes, $fake$.



(a) AlexNet_p. (Left) CIFAR10, (b) ResNet_p-18. (Left) CIFAR10, (Right) CIFAR100.

Fig. 12: Ambiguity Attack: Classification accuracy of our passport networks with valid passport, *random attack* ($fake_1$) and *reversed-engineering attack* ($fake_2$) on CIFAR10 and CIFAR100. Note that, the accuracies of our passport networks with valid passports and original DNN (without passport) are too close to separate in histograms.

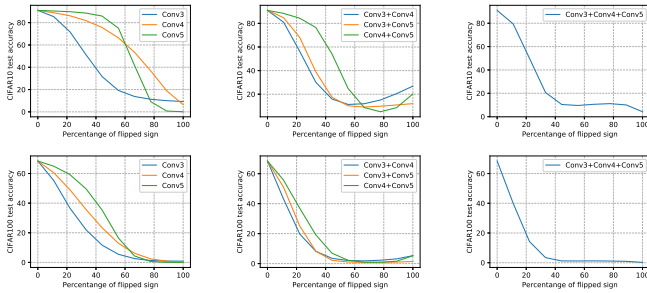


Fig. 13: Ambiguity Attack (Random): It can be seen that the performance of AlexNet_p deteriorates with randomly flipped scale factor signs. Left to right: flip one layer, two layers and three layers, respectively. Top row is CIFAR10 and bottom row is CIFAR100 dataset.

performances by using fake passports, regardless of the fake passports are either randomly generated or reverse-engineered with the use of original training datasets. Table VII summarize the accuracy of the proposed methods under ambiguity attack modes, $fake$ depending on attackers' knowledge of the protection mechanism. It shows that all the corresponding passport-based DNN models accuracies are deteriorated to various extents. The ambiguous attacks are therefore defeated according to the fidelity evaluation process, $F()$. We'd like to highlight that even under the most adversary condition, i.e.

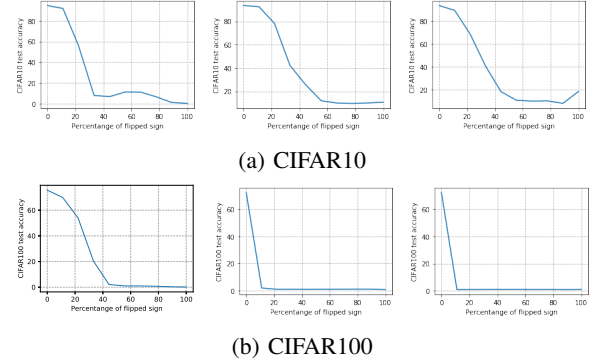
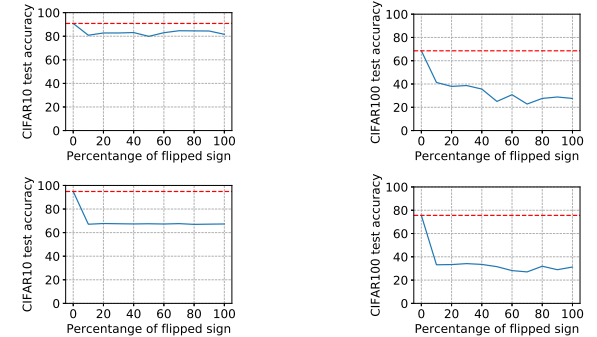


Fig. 14: ResNet_p-18: It can be seen that the performance deteriorates with randomly flipped scale factor signs. Left to right: Scheme \mathcal{V}_1 , \mathcal{V}_2 and \mathcal{V}_3 , respectively.



(a) CIFAR10 (top: AlexNet_p; bot- tom: ResNet_p-18) (b) CIFAR100 (top: AlexNet_p; bottom: ResNet_p-18)

Fig. 15: Performance of (a) CIFAR10 and (b) CIFAR100 when adversaries try to forge a new signature by a certain % of dissimilarity ϵ_f with the original signature.

freezing weights, maximizing the distance from the original passport P , and minimizing the accuracy loss (in layman terms, it means both the original passports and scale signs are exploited due to insider threat, and we class this as $fake_3$), attackers are still unable to use new (modified) scale signs without compromising the network accuracies. As shown in Fig. 16, with 10% and 50% of the original scale signs are modified, the CIFAR100 classification accuracy drops about 5% and 50%, respectively. In case that the original scale sign remains unchanged, the DNN model ownership can be easily verified by the pre-defined string of signs. Also, Table VII shows that attackers are unable to exploit D_t to forge ambiguous passports.

Based on these empirical studies, we decide to set the threshold ϵ_f in Definition 1 as 3% for AlexNet_p and 20% for

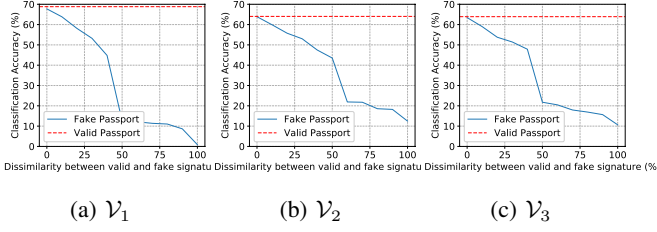


Fig. 16: Ambiguity Attack: Classification accuracy on CIFAR100 under insider threat ($fake_3$) on three verification schemes. It is shown that when a correct signature is used, the classification accuracy is intact, while for a partial correct signature (sign scales are modified around 10%), the performance will immediately drop around 5%, and a totally wrong signature will obtain a meaningless accuracy (1-10%). Based on the threshold $\leq \epsilon_f = 3\%$ for AlexNet_p and by the fidelity evaluation process F , any potential ambiguity attacks (even with partially correct signature) are effectively defeated.

Learned Parameters		Signature s	
Scale factor γ	sign (+/-)	ASCII code	Character
-0.1113	-1	116	t
0.2344	1		
0.2494	1		
0.4885	1		
-0.1021	-1		
0.3889	1		
-0.1225	-1	104	h
-0.3401	-1		
-0.1705	-1		
0.3338	1		
0.1884	1		
-0.1215	-1		
0.1620	1	105	i
-0.1754	-1		
-0.2698	-1		
-0.1958	-1		
-0.1007	-1		
0.3923	1		
0.4288	1	115	s
-0.1125	-1		
0.4355	1		
-0.1524	-1		
-0.1073	-1		
0.1922	1		

TABLE VIII: Sample of the learned scale factor γ and respective signs (+/-) from the 48 out of 256 channels from Conv5 of AlexNet_p when we embed signature $s = \{\text{this}\}$ and $\{\text{is}\}$.

Learned Parameters		Signature s	
Scale factor γ	sign (+/-)	ASCII code	Character
-0.1657	-1	105	i
0.1665	1		
0.4633	1		
-0.2668	-1		
0.3830	1		
-0.1789	-1		
-0.1077	-1	115	s
0.1585	1		
-0.2257	-1		
0.2916	1		
0.2169	1		
0.1862	1		

	Signature s	Accuracy (%)
AlexNet (baseline)	-	91.12
AlexNet _p	<i>this is an example signature</i>	90.89
	<i>thhs iB an xxxpxX siggature</i>	82.83
	<i>qpCA2J^OEcΔo * 1ay</i>	11.44

TABLE IX: A comparison of the accuracy of AlexNet(s) in CIFAR10 classification task when a correct (top), partially correct (middle) or totally wrong (bottom) signature is used.

$s = \{\text{this is an example signature}\}$ into the Conv5 of AlexNet_p by using sign loss (Eq. 6). Note that the maximum size of an embedded signature is depending on the number of the channels in a DNN model. For instance, in this paper, the Conv5 of AlexNet_p as shown in Table III has 256 channels, so the maximum signature capacity can be embedded is 256bits.

For ownership verification, the embedded signature s can be revealed by decoding the learned sign of scale factors. For example, in Table VIII, every 8bits of the scale factor sign is decoded into ASCII code as follow:

1. $\{-1, 1, 1, 1, -1, 1, -1, -1\} \rightarrow 116 \rightarrow t$
2. $\{-1, 1, 1, -1, 1, -1, -1, -1\} \rightarrow 104 \rightarrow h$
3. $\{-1, 1, 1, -1, 1, -1, -1, -1\} \rightarrow 105 \rightarrow i$
4. $\{-1, 1, 1, 1, -1, -1, 1, 1\} \rightarrow 115 \rightarrow s$
5. $\{-1, 1, 1, -1, 1, -1, -1, 1\} \rightarrow 105 \rightarrow i$
6. $\{-1, 1, 1, 1, -1, -1, 1, 1\} \rightarrow 115 \rightarrow s$

Note that, in this proposed method, similar character (e.g. $\{i\}$ and $\{s\}$) appears in different position of a string will have different scale factors. Table IX shows a comparison result when a correct signature, partial correct signature or total wrong signature is used in CIFAR10 classification task with AlexNet_p. It is shown that when a correct signature is used (i.e. this is an example signature), the classification accuracy reached 90.89%, while for a partial correct signature, the performance is dropped to 82.23%, and a totally wrong signature will obtain a meaningless accuracy (11.44%). Based on the threshold $\epsilon_f = 3\%$ for AlexNet_p and by the fidelity evaluation process, any potential ambiguity attacks (even with partially correct signature) are effectively defeated.

F. Network Complexity

Table X shows the training and inference time of each scheme on AlexNet_p and ResNet_p-18, respectively using one NVIDIA Titan V. In both of the proposed DNN architectures, the inference time of the baseline, scheme \mathcal{V}_2 , scheme \mathcal{V}_3 are almost the same as to the execution time because all of them didn't use passport to calculate γ and β . However, scheme \mathcal{V}_1 is slightly slower (about 10%) compared to the baseline because of the extra computational cost of γ and β calculation from the passport. Training time of scheme \mathcal{V}_1 , scheme \mathcal{V}_2 and scheme \mathcal{V}_3 are slower than the baseline about 18%(ResNet_p-18)/27%(AlexNet_p), 116%(ResNet_p-18)/125% and 127%(ResNet_p-18)/153%, respectively. Scheme \mathcal{V}_2 and scheme \mathcal{V}_3 are slower about 2x than scheme \mathcal{V}_1 due to the multi task training scheme. Nonetheless, we tested a larger network (i.e. ResNet_p-50) and its training time increases 10%, 182% and 191% respectively for \mathcal{V}_1 , \mathcal{V}_2 and \mathcal{V}_3 schemes. This

ResNet_p-18, respectively. By this fidelity evaluation process, any potential ambiguity attacks are effectively defeated. In summary, extensive empirical studies have shown that it is impossible for adversaries to maintain the original DNN model accuracies by using counterfeit passports, regardless of they are either randomly generated or reverse-engineered with the use of original training datasets. This passport dependent performances play an indispensable role in designing secure ownership verification schemes that are illustrated in Sect. III-D.

E. Sign of scale factors as signature

In this section, we show how the sign (+/-) of scale factor γ can be used to encode a signature s such as ASCII code. Table VIII shows an example of the learned scale factors and its respective sign when we embed a signature

	CIFAR10	
	T	I
AlexNet (Baseline)	8.445	0.834
AlexNet _p \mathcal{V}_1	10.745	0.912
AlexNet _p \mathcal{V}_2	19.010	0.830
AlexNet _p \mathcal{V}_3	21.372	0.881

	CIFAR10	
	T	I
ResNet (Baseline)	31.09	1.71
ResNet _p -18 \mathcal{V}_1	36.67	1.94
ResNet _p -18 \mathcal{V}_2	67.21	1.87
ResNet _p -18 \mathcal{V}_3	70.69	1.88

TABLE X: Training (T) and Inference (I) time of each scheme on AlexNet_p (left) and ResNet_p-18 (right) using one *NVIDIA Titan V*. The values are in seconds/epoch.

	Scheme \mathcal{V}_1	Scheme \mathcal{V}_2	Scheme \mathcal{V}_3
Training	- Passport layers added - Passports needed - 15%-30% more training time	- Passport layers added - Passports needed - 100%-125% more training time	- Passport layers added - Passports & Trigger set needed - 100%-150% more training time
Inferencing	- Passport layers & Passports needed - 10% more inferencing time	- Passport layers & Passport NOT needed - NO extra time incurred	- Passport layers & Passport NOT needed - NO extra time incurred
Verification	- NO separate verification needed	- Passport layers & Passports needed	- Trigger set needed (black-box verification) - Passport layers & Passports needed (white-box verification)

TABLE XI: Summary of our proposed passport networks complexity for \mathcal{V}_1 , \mathcal{V}_2 and \mathcal{V}_3 schemes.

increase is consistent with those smaller models i.e. AlexNet_p and ResNet_p-18.

Table XI summarizes the complexity of passport networks in various schemes. We believe that it is the computational cost at the inference stage that is required to be minimized, since network inference is going to be performed frequently by the end users. While extra costs at the training and verification stages, on the other hand, are not prohibitive since they are performed by the network owners, with the motivation to protect the DNN model ownerships.

V. DISCUSSIONS AND CONCLUSIONS

Considering billions of dollars have been invested by giant and start-up companies to explore new DNN models virtually every second, we believe it is imperative to protect these inventions from being stolen. While ownership of DNN models might be resolved by registering the models with a centralized authority, it has been recognized that these regulations are inadequate and technical solutions are urgently needed to support the law enforcement and juridical protections. It is this motivation that highlights the unique contribution of the proposed method in unambiguous verification of DNN models ownerships.

Methodology-wise, our empirical studies re-asserted that over-parameterized DNN models can successfully learn multiple tasks with arbitrarily assigned labels and/or constraints. While this assertion has been theoretically proved [15] and empirically investigated from the perspective of network generalization [16], its implications to network security in general remain to be explored. We believe the proposed modulation of DNN performance based on the presented passports will play an indispensable role in bringing DNN behaviours under control against adversarial attacks, as it has been demonstrated for DNN ownership verifications.

ACKNOWLEDGEMENT

This research is partly supported by the Fundamental Research Grant Scheme (FRGS) MoHE Grant FP021-2018A, from the Ministry of Education Malaysia. Also, we gratefully

acknowledge the support of NVIDIA Corporation with the donation of the Titan V GPU used for this research.

REFERENCES

- [1] Y. Uchida, Y. Nagai, S. Sakazawa, and S. Satoh, "Embedding watermarks into deep neural networks," in *ICMR*, 2017, pp. 269–277.
- [2] Y. Adi, C. Baum, M. Cisse, B. Pinkas, and J. Keshet, "Turning your weakness into a strength: Watermarking deep neural networks by backdoor," in *USENIX*, 2018, pp. 1615–1631.
- [3] H. Chen, B. Darvish Rohani, and F. Koushanfar, "DeepMarks: A Digital Fingerprinting Framework for Deep Neural Networks," *arXiv preprint arXiv:1804.03648*, 2018.
- [4] J. Zhang, Z. Gu, J. Jang, H. Wu, M. P. Stoecklin, H. Huang, and I. Molloy, "Protecting intellectual property of deep neural networks with watermarking," in *ASIACCS*, 2018, pp. 159–172.
- [5] B. Darvish Rouhani, H. Chen, and F. Koushanfar, "DeepSigns: A Generic Watermarking Framework for IP Protection of Deep Learning Models," *arXiv preprint arXiv:1804.00750*, 2018.
- [6] E. Le Merrer, P. Perez, and G. Trédan, "Adversarial Frontier Stitching for Remote Neural Network Watermarking," *arXiv preprint arXiv:1711.01894*, 2017.
- [7] G. Jia and M. Potkonjak, "Watermarking deep neural networks for embedded systems," in *ICCAD*, 2018, pp. 1–8.
- [8] Q. Li and E.-C. Chang, "Zero-knowledge watermark detection resistant to ambiguity attacks," in *Proceedings of the 8th workshop on Multimedia and security*, 2006, pp. 158–163.
- [9] H. T. Sencar and N. D. Memon, "Combating ambiguity attacks via selective detection of embedded watermarks," *IEEE Trans. Information Forensics and Security*, vol. 2, no. 4, pp. 664–682, 2007.
- [10] S. Craver, N. Memon, B. . Yeo, and M. M. Yeung, "Resolving rightful ownerships with invisible watermarking techniques: limitations, attacks, and implications," *IEEE Journal on Selected Areas in Communications*, vol. 16, no. 4, pp. 573–586, 1998.
- [11] Y. Wu and K. He, "Group normalization," in *Proceedings of the European Conference on Computer Vision (ECCV)*, 2018, pp. 3–19.
- [12] S. Ioffe and C. Szegedy, "Batch normalization: Accelerating deep network training by reducing internal covariate shift," in *ICML*, 2015, pp. 448–456.
- [13] K. He, X. Zhang, S. Ren, and J. Sun, "Delving deep into rectifiers: Surpassing human-level performance on imagenet classification," in *Proceedings of the IEEE International Conference on Computer Vision (ICCV)*, 2015, pp. 1026–1034.
- [14] A. See, M.-T. Luong, and C. D. Manning, "Compression of neural machine translation models via pruning," in *Proceedings of The 20th SIGNLL Conference on Computational Natural Language Learning*, 2016, pp. 291–301.
- [15] Z. Allen-Zhu, Y. Li, and Z. Song, "A convergence theory for deep learning via over-parameterization," in *ICML*, 2019, pp. 242–252.
- [16] C. Zhang, S. Bengio, M. Hardt, B. Recht, and O. Vinyals, "Understanding deep learning requires rethinking generalization," *arXiv preprint arXiv:1611.03530*, 2016.